Electronic configuration of the c(2 × 2)MnCu two-dimensional alloy in layered structures supported on Cu(100)

2003 J. Phys.: Condens. Matter 15 1183

(http://iopscience.iop.org/0953-8984/15/8/304)

INSTITUTE OF PHYSICS PUBLISHING JOURNAL OF PHYSICS: CONDENSED MATTER

J. Phys.: Condens. Matter **15** (2003) 1183–1200 PII: S0953-8984(03)55732-0

Electronic configuration of the c(2 × 2)MnCu two-dimensional alloy in layered structures supported on Cu(100)

S Gallego[1], M C Muñoz[1], Y Huttel[1,2,3], J Avila[1,2] and M C Asensio[1,2]

[1] Instituto de Ciencia de Materiales de Madrid, Consejo Superior de Investigaciones Científicas, Cantoblanco, 28049 Madrid, Spain
[2] LURE, Bâtiment 209D, Centre Universitaire Paris-Sud, 91405 Orsay, France

E-mail: icmsg03@pinar2.csic.es (S Gallego)

Received 7 November 2002
Published 17 February 2003
Online at stacks.iop.org/JPhysCM/15/1183

Abstract

The c(2 × 2)MnCu surface alloy on Cu(100) can be considered as a purely two-dimensional magnetic system where the Mn atoms exhibit a large corrugation closely related to their high spin moment. In this paper we investigate the influence of the atomic environment on the electronic and magnetic properties of the two-dimensional alloyed layer, extending our study to the less known multilayered system made of MnCu two-dimensional alloy layers embedded in a Cu crystal. The analysis is based on angle-resolved photoelectron spectroscopy measurements and calculations using the Green function matching method, which allows us to treat exactly the projection of the three-dimensional lattice on the c(2 × 2) plane. A complete study of the valence band is performed along the two-dimensional Brillouin zone in a wide energy range. We show that the presence of Mn results in an important redistribution of the spin-polarized electronic states of the neighbouring Cu atoms. This redistribution is not accompanied by a net charge transfer between different atoms, and also the spin moment of Cu remains small. Most of the new features induced by Mn in the surface alloy are also present in the multilayered system, evidencing that they are specific to the two-dimensional alloyed layer and not surface effects.

1. Introduction

The c(2 × 2)MnCu/Cu(100) surface alloy has attracted considerable attention in the last decade [1–13]. It is formed by the room temperature deposition of 0.5 ML (monolayers) of Mn on Cu(100). The Mn and Cu atoms of the topmost plane arrange in a chequerboard

[3] Present address: Instituto de Microelectrónica de Madrid, Consejo Superior de Investigaciones Científicas, Isaac Newton 8,Tres Cantos, 28760 Madrid, Spain.

structure, where the Mn atoms occupy substitutional adsorption sites with a large outward corrugation of ∼0.3 Å. The origin of this unusually high buckling has been attributed to the high local magnetic moment of Mn [7, 14]. From different experimental and theoretical studies of the electronic structure of the system [9–12, 15–17], it has been found that the minority-spin d band of Mn is almost unoccupied, and completely separated from the occupied majority-spin band. Also measurements using soft-x-ray absorption spectroscopy (SXAS) clearly indicate that the Mn atoms are in a high-spin ground state [7, 8, 11]. The majority-spin band of Mn overlaps in energy the valence band of Cu, and as a result, few new states induced by Mn have been identified until now. This is also partly due to the methods used to calculate the electronic structure of this system. The rigorous *ab initio* techniques that have been applied are computationally very demanding, which forces the use of slab models. These models introduce an artificial discretization of the bulk projection along the normal to the surface, making the identification of the surface features difficult. The Green function matching method on which we base our analysis takes into account properly the projection of the semiinfinite bulk onto the plane of the surface, and naturally provides the electronic structure layer by layer. In a previous article [12], we have already shown that new features not overlapping the bulk projection can be identified in the region close to E_F and around the point $\overline{\mathrm{M}}$. This was later confirmed by a different group [18]. The surface localization of these states was determined even without considering the buckling of the Mn atoms.

The atomic environment of Mn has a relevant influence on the establishment of the long-range magnetic properties. Different theoretical studies predict the ferromagnetic configuration as the ground state of the surface alloy [3, 9, 19], and very recently a phase transition from a paramagnetic to a ferromagnetic state has been observed at 50 ± 5 K by x-ray magnetic circular dichroism (XMCD) [20]. Theoretical calculations of the electronic structure of an ideal corrugated c(2 × 2)MnCu bilayer predict in-plane ferromagnetism, while the coupling between the two CuMn layers is antiferromagnetic [10]; however, these results depend strongly on the effective volume of the Mn atoms. In the present contribution we analyse in detail the effects of the atomic environment of Mn on the electronic structure and magnetic moments of the c(2 × 2)MnCu two-dimensional alloy, both as a surface layer on Cu(100) and as a layer embedded in a Cu matrix. Special attention is paid to the effects of the corrugation of the CuMn plane.

The organization of the paper is as follows. In section 2 we explain the details of the methods used in our study, namely calculations within the Green function matching formalism and measurements using angle-resolved ultraviolet photoemission spectroscopy (ARUPS). The electronic structure of the c(2 × 2)MnCu/Cu(100) surface is presented in section 3, analysing the changes induced by the presence of Mn with respect to the (1 × 1)Cu(100) termination. Section 4 is devoted to the effects of embedding the MnCu alloyed layer in Cu and the formation of multilayered structures by the repetition of the c(2 × 2)MnCu/Cu(100) sequence. The conclusions are summarized in section 5.

2. Method of analysis

2.1. Theoretical method

Our calculations are based on a tight-binding model within the Slater–Koster parametrization scheme [21], using orthogonal parameters with interactions up to the second-nearest neighbours. The effective parameters were derived from those corresponding to the paramagnetic elements [22]. To properly describe the spin magnetism of Mn, we added an exchange potential obtained adjusting the exchange splitting and the magnetic moments

Table 1. Tight-binding matrix elements (in eV) for the spin-polarized Mn and the Cu atoms in a MnCu layer (denoted Mn and Cu_0, respectively), the neighbouring Cu atoms of the adjacent substrate layer (Cu_1) and the Cu atoms in a pure Cu crystal. All interatomic distances refer to the ideal positions of an fcc Cu lattice: 2.55 Å for 1NN (first-nearest neighbours) and 3.61 Å for 2 NN. No difference due to the spin polarization or the layer position is assumed in the hopping integrals.

On-site	Mn (major)	Mn (minor)	Cu_0	Cu_1	Cu
E_s	12.3728	12.9171	10.8120	10.8120	10.8120
E_p	17.9097	18.6104	18.4156	18.4156	18.4156
E_{d1}	4.5225	8.6807	4.3759	4.6759	5.0759
E_{d2}	4.3914	8.5496	4.3586	4.6586	5.0586
	1NN		2NN		
Hopping	Mn–Cu	Cu–Cu	Mn–Mn	Mn–Cu	Cu–Cu
(ssσ)	−1.1134	−1.0229	−0.0574	−0.0268	−0.0125
(spσ)	1.6606	1.5743	0.2456	0.2020	0.1661
(sdσ)	−0.5197	−0.4227	−0.1577	−0.1352	−0.1159
(ppσ)	2.6946	2.6761	0.8042	0.7679	0.7332
(ppπ)	0.1620	0.2640	0.0430	0.0703	0.1151
(pdσ)	−0.5945	−0.4475	−0.1936	−0.1188	−0.0729
(pdπ)	0.2825	0.2385	0.0620	0.0521	0.0437
(ddσ)	−0.4750	−0.3491	−0.0935	−0.0757	−0.0614
(ddπ)	0.3261	0.2449	0.0401	0.0363	0.0328
(ddδ)	−0.0718	−0.0555	0.0004	−0.0013	−0.0039

to previous *ab initio* values from calculations within the local density approximation [9, 10]. The hopping interaction between Mn and Cu was defined as the geometrical average of the single-element terms. The resulting interaction matrix elements are presented in table 1. The asymmetry introduced by the highly corrugated MnCu layer was taken into account through the scaling law relating the hopping terms $V_{ll'm}^{A,B}$ and the interatomic distance d:

$$V_{ll'm}^{A,B} = C_{ll'm}^{A,B} d^{-(l+l'+1)} \tag{1}$$

where A, B refer to the chemical species, C is the characteristic coefficient to be determined, and l, l', m label the angular momentum quantum numbers of the orbitals involved [23].

The layered structures were modelled using the surface Green function matching method [24]. Within this formalism, the Green function of the semiinfinite surface/interface system can be expressed exactly in terms of the coupling interactions of the constituent layers and the projections on the surface/interface domain of the bulk Green function. A redistribution of charge at the topmost layers is allowed, adding a surface potential to preserve the total charge neutrality of the system. In table 2 we give the chemical- and orbital-dependent surface potentials used in our calculations, both for the c(2 × 2) surface alloy and for the (1 × 1)Cu(100) termination.

2.2. Experimental procedure

The experiments were carried out in the Spanish–French beamline at LURE (*Laboratoire pour l'Utilisation du Rayonnement Électromagnétique*, Orsay), receiving synchrotron radiation from the SU8 insertion device of the SuperAco storage ring. All the data were taken at room temperature. The ultra-high-vacuum (UHV) chamber, of base pressure 2×10^{-10} mbar, was equipped with a high-precision (better than 1°) manipulator allowing rotation along the

Table 2. Orbital- and atomically resolved surface potential (in eV) at the Cu(100) and the c(2 × 2)MnCu/Cu(100) surfaces. The negative sign indicates an attractive potential. The subindices of the elements refer to the corresponding layer, numbered from the surface (layer 0) to the bulk.

	Cu(100)		c(2 × 2)MnCu	
Atom	sp	d	sp	d
Mn_0	—	—	−0.45	−0.29
Cu_0	−1.40	0.10	−1.50	0.10
Cu_1	−0.24	0.00	−0.20	−0.20

azimuthal and polar angles. In addition, a LEED (low-energy electron diffraction) acquisition data-system was operative in the vacuum chamber.

The Cu(100) single crystal used as substrate was cleaned by repeated cycles of Ar^+ bombardment followed by annealing at 450 °C. Afterwards, the surface showed a sharp p(1 × 1) LEED pattern, and no traces of contaminants were detected in the core level or valence band photoemission spectra. To form the c(2 × 2)MnCu superstructure, 0.5 ML of Mn (99.98%) were evaporated from a resistively heated ceramic crucible. The evaporation rate of 0.9 ± 0.1 ML min^{-1} was monitored by a quartz balance. This surface was used as the starting point to create a second c(2 × 2)MnCu/Cu(100) sequence. For this purpose, after checking the cleanliness and quality of the surface alloy, Cu (99.999%) was deposited from a tungsten filament covered by Cu, at an evaporation rate of 2 ML min^{-1}. Increasing the amount of Cu resulted in a weakening of the c(2 × 2) LEED pattern, and for coverages $\geqslant$ 4 ML a (1 × 1) symmetry developed. Additional Cu exposure sharpened the (1 × 1) pattern, with a very low background intensity for deposits of 10 ML. A new MnCu surface alloy was formed on top following the procedure described above. During all the evaporations the pressure remained below 10^{-9} mbar.

The measurements of the valence band structure were performed using linearly polarized synchrotron radiation. A careful alignment of the sample was done by LEED and refined by photoelectron diffraction (PhD), combining polar cuts in a high-symmetry direction with azimuthal cuts at 45° off normal. The angle-resolved photoemission spectra were recorded along the main symmetry lines of the corresponding surface (cf figure 1), using a photon energy of 32 eV. For the clean substrate and the Cu-ended surfaces, the unit cell corresponds to the ideal (1 × 1) cut of the (100) crystal. The existence of two inequivalent sites at the MnCu layer leads to the reduced c(2 × 2) BZ (Brillouin zone) in the surface alloy. All measured spectra presented here are referred to the symmetry lines of the (1 × 1) unit cell.

3. The c(2 × 2)MnCu/Cu(100) surface alloy

The starting point of all our further analysis is the description of the electronic structure of Cu(100). The valence band of bulk Cu is dominated by the completely filled 3d states, which extend mainly from −5 to −2 eV below the Fermi level (E_F), the highest occupancies corresponding to energies above −4 eV. The d band is weakly hybridized to the sp band, although the spectral weight of the sp states becomes relevant only at the bottom of the valence band and over E_F. This structure is preserved at the (100) surface. The Cu(100) surface has been largely studied in the last decades [25–29], and it is considered to be well characterized. In figure 2 we show the density of states (DOS) of the topmost layer and the bulk projected along the high-symmetry lines of the two-dimensional BZ. Due to the screened interaction in

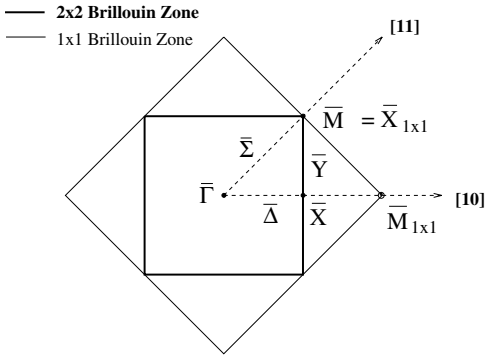

Figure 1. Scheme of the first BZ of the c(2 × 2)MnCu/Cu(100) surface, labelling the three main symmetry points ($\overline{\Gamma}$, $\overline{X}$, $\overline{M}$) and lines ($\overline{\Delta}$, $\overline{Y}$, $\overline{\Sigma}$). Also shown is the BZ of the (1 × 1) unit cell, the corresponding symmetry points being denoted by the subindices (1 × 1).

metals, the surface effects are almost confined to the two outermost atomic planes. They consist in a slight narrowing of the DOS, and the existence of some surface states (SSs) and surface resonances (SRs) in specific directions of the BZ. Large gaps of the bulk projection occur close to E_F around the point $\overline{M}$, and bulk pockets can be identified between −5 and −3 eV along the high-symmetry lines [29]. SSs appear in almost all these gaps and pockets, preferentially close to edges of the bulk projection, and some of them evolve into SRs. As a reference, the main SSs identified for Cu(100) at the high-symmetry points are summarized in table 3. Our results are in good agreement with the previous theoretical and experimental data, although the state $\overline{M}_1$, which converts into an SS only when relativistic effects are included [28], is solved here as an SR. The theoretical dispersion along $\overline{\Delta}$ and $\overline{\Sigma}$ can be compared to the ARUPS results of figure 3. Two main subbands can be identified at $\overline{\Gamma}$ in figure 2. The upper one, extending between −4 and −2 eV, is clearly observed in the spectra. It broadens as it disperses along $\overline{\Delta}$, and becomes narrower along $\overline{\Sigma}$; close to $\overline{X}$ it hybridizes to the sp band crossing E_F. The lower subband, centred around −5 eV, is not detected in the experiments at $\overline{\Gamma}$. It hybridizes to the upper one near $\overline{X}$. Along $\overline{\Sigma}$, both subbands also hybridize close to the middle point, and then separate again into two structures towards $\overline{M}$, the lower one overlapping the bottom s band. The theoretical dispersion is compatible with the spectra regarding the selection rules of photoemission: in the experiments, the polarization vector of the incident light is contained in the plane of emission, and as a result only even states under mirror reflection around this plane can be detected. According to our calculations, the d states below −4 eV exhibit odd mirror symmetry; only when they hybridize to the even d states of higher energy do they contribute to the photoemission transitions.

When the MnCu surface alloy is formed on top of the Cu(100) surface, the two-dimensional symmetry changes. As a consequence, the actual BZ of the bulk is folded onto the reduced (2 × 2) unit cell, resulting in the overlap of symmetry inequivalent projections from the bulk and the reduction of the effective bulk bandgaps. In addition, the presence of a different chemical element with a strong spin polarization induces new features in the DOS. In figure 4 we present the spin-resolved DOS along the symmetry lines of the c(2 × 2)MnCu surface, assuming a buckling of 0.3 Å of the Mn atoms and a ferromagnetic configuration. Figures 4(a)–(c) correspond respectively to the DOS at the Mn and Cu sites of the topmost layer (layer 0), and to the bulk projection. Although not shown here, from layer 2 on the DOS remained very similar to that of the bulk, layer 1 being a transition layer between the topmost Cu (Cu_0) and the bulklike Cu atoms. It is evident from the figure that the Mn atoms exhibit a strong spin splitting,

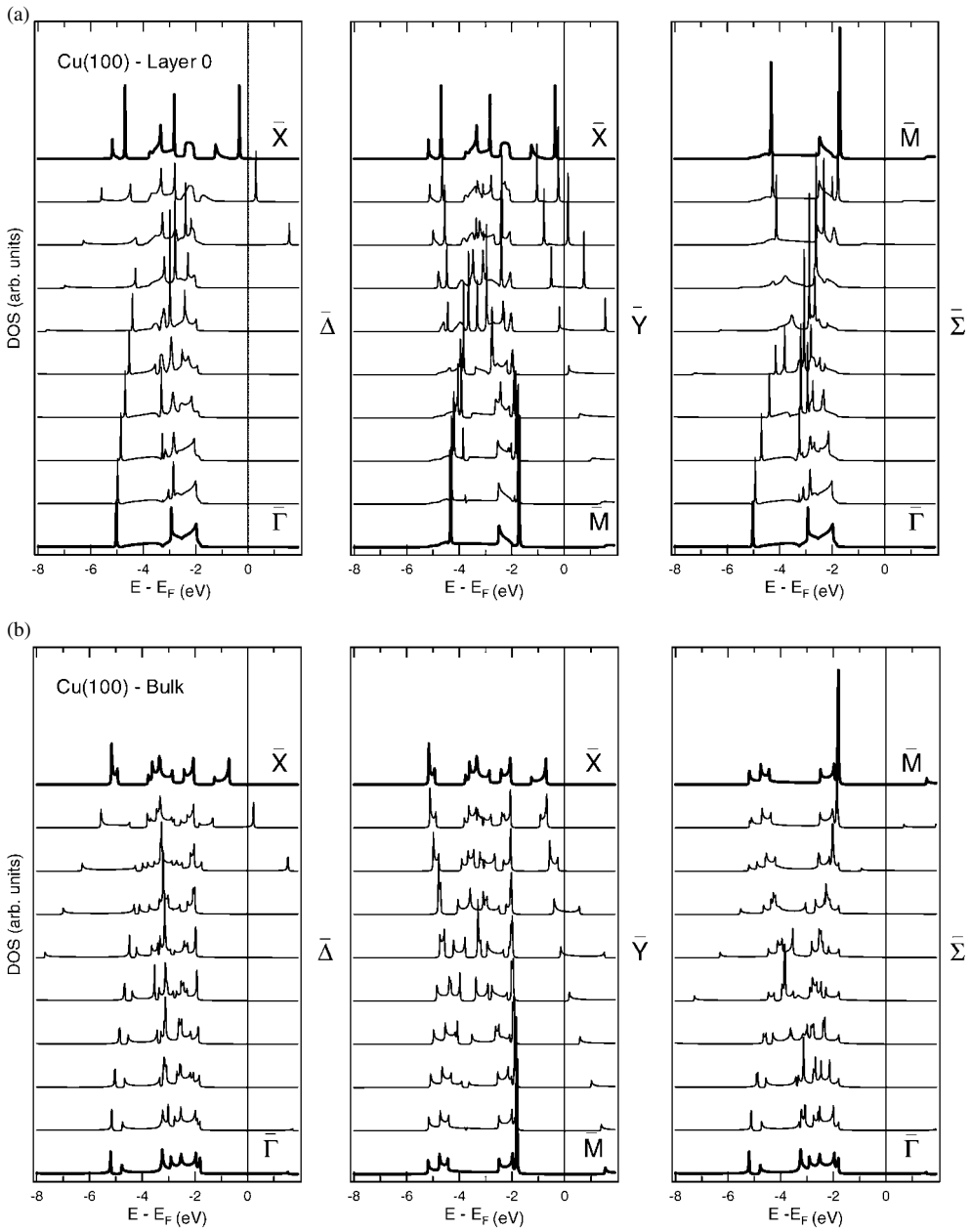

Figure 2. *k*-resolved DOS of the (1×1)Cu(100) surface. The three upper panels (a) correspond to the outermost layer (layer 0), and the lower ones (b) to the bulk projection. Each panel represents the dispersion along one of the high-symmetry lines of the surface BZ, the curves corresponding to the high-symmetry points being indicated.

the minority-spin states lying essentially in the conduction band. Both the localization in energy of the conduction band and the exchange splitting of approximately 4.5 eV, evaluated from the integrated DOS, are in agreement with previous theoretical values[10]. Angle resolved

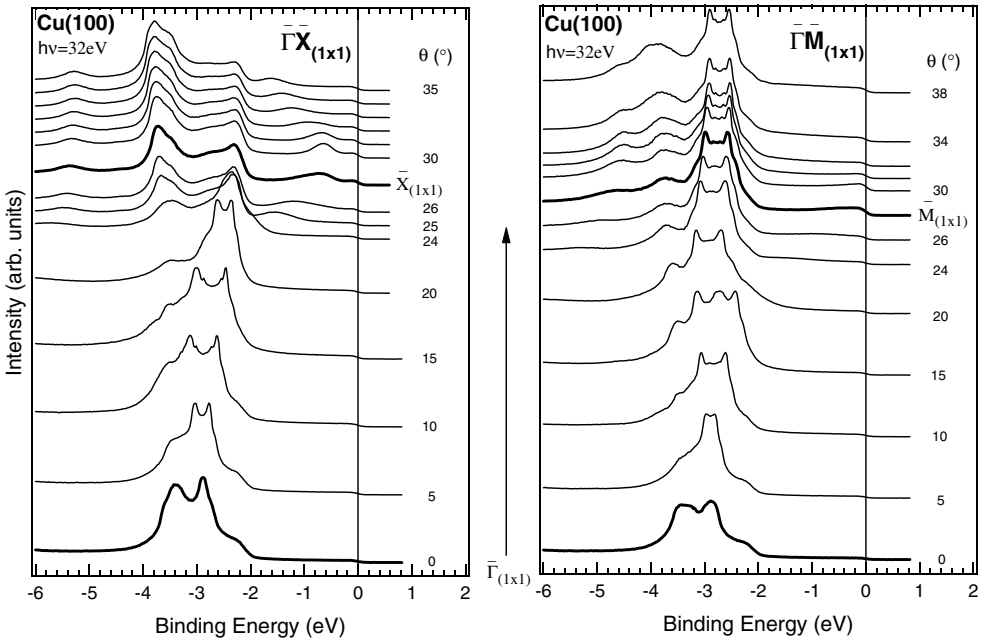

Figure 3. ARUPS spectra of the clean (1 × 1)Cu(100) surface along the directions $\overline{\Delta}$ and $\overline{\Sigma}$ of the (1 × 1) BZ. A step of 1° in the polar angle roughly corresponds to a step of 0.04 Å^{-1} in $k_{\|}$. The spectra corresponding to the high-symmetry points are indicated. The energy is referred to the Fermi level of Cu.

Table 3. Main SSs of the (1 × 1)-Cu(100) surface, indicating their position in electron volts with respect to E_F at the corresponding symmetry point. The previous experimental and theoretical values shown on the right have been taken from the references indicated in brackets. See the text for details.

State	This work	Exp.	Theory
$\overline{\Gamma}_1$	−5.02	−5.15 [26]	−4.7 [29]
$\overline{X}_1$	−0.34	−0.06 [26]	−0.31 [27]
$\overline{X}_3$	−4.69	−4.62 [26]	−4.4 [29]
$\overline{M}_1$	−2.74	−2.11 [28]	−1.77 [27]
$\overline{M}_2$	−1.71	−1.81 [30]	−1.3 [29]

inverse photoemission measurements [9, 31] have identified the unoccupied minority band of Mn above 1.8 eV from E_F, which results in a exchange splitting of 5.5 eV; however, this much larger experimental value was assigned to the excitation Coulomb energies involved in the photoemission process [9]. Furthermore, recent experimental investigations based on the symmetry of the BZ have led to an experimental value of 4.85 eV for the exchange splitting [32]. There is a strong hybridization of the majority-spin d bands of Mn and Cu, which also exhibit almost the same bandwidth in the total DOS. This induces a spin polarization of the Cu atoms which are closer to Mn; consequently, the distribution of the Cu states is very different for both spin directions, even if the quantitative difference in occupation between them is not very high, as we will show later. In contrast, the minority d band of Mn does not overlap that of Cu, and as a consequence the hybridization is lowered and the bandwidth reduced. The conduction band is dominated by the minority-spin d orbitals of Mn, which form a narrow band of width around

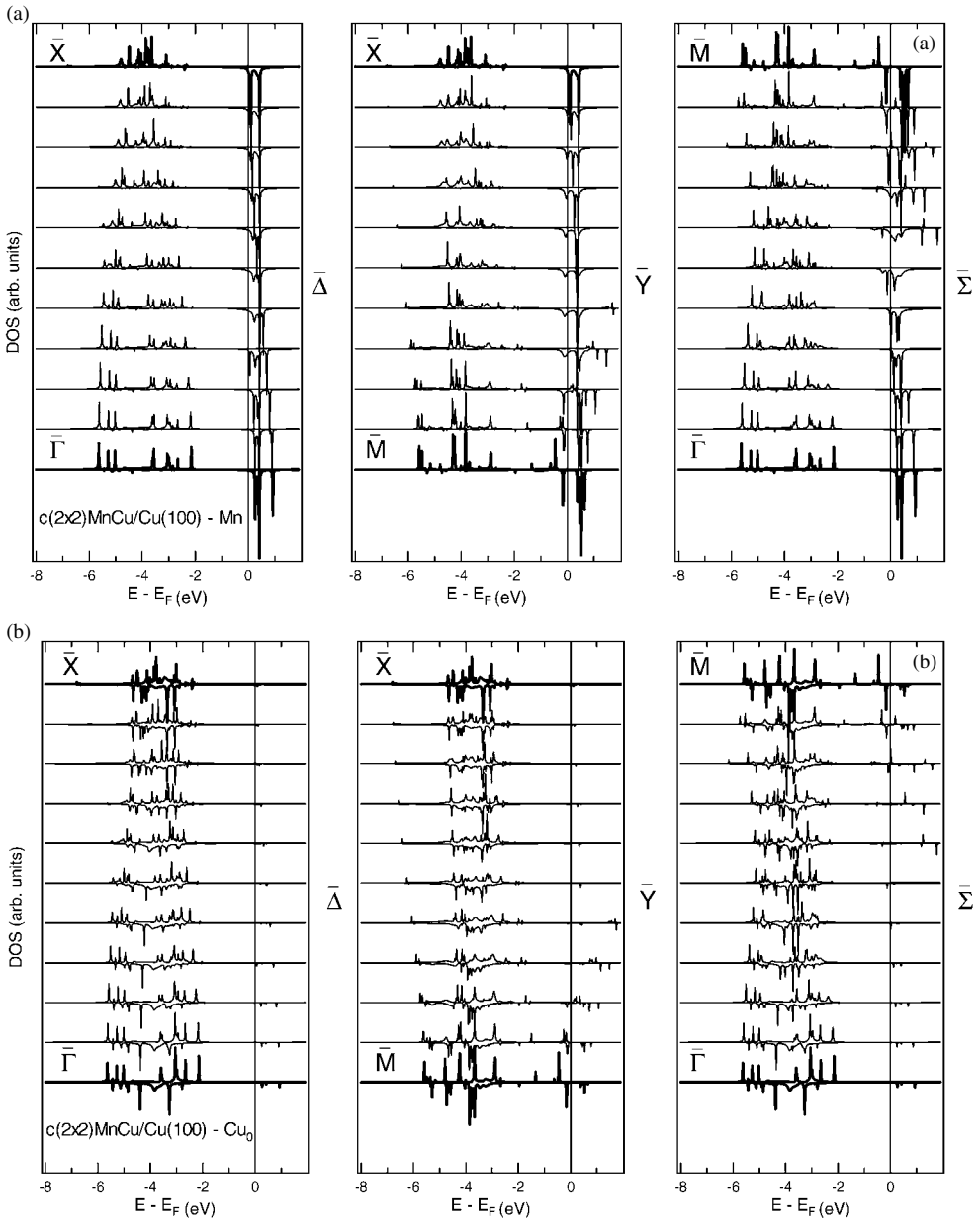

Figure 4. Spin- and k-resolved DOS of the c(2×2)MnCu/Cu(100) surface at (a) the Mn site, (b) the Cu site (Cu_0) of the topmost MnCu layer and (c) the bulk projection. Each panel represents the dispersion along one of the high-symmetry lines of the (2×2) unit cell. The positive (negative) curves correspond to the majority (minority) spin projections.

1 eV centred between 0.4 and 0.6 eV. This band hybridizes the bulk sp band when it crosses the Fermi level near $\overline{\mathrm{M}}$. In this sense the spin polarization of the Cu_0 states in the conduction band is a hint of their origin: when they are induced by the hybridization to Mn they belong to the minority-spin band, while the majority-spin states are characteristic of the Cu lattice.

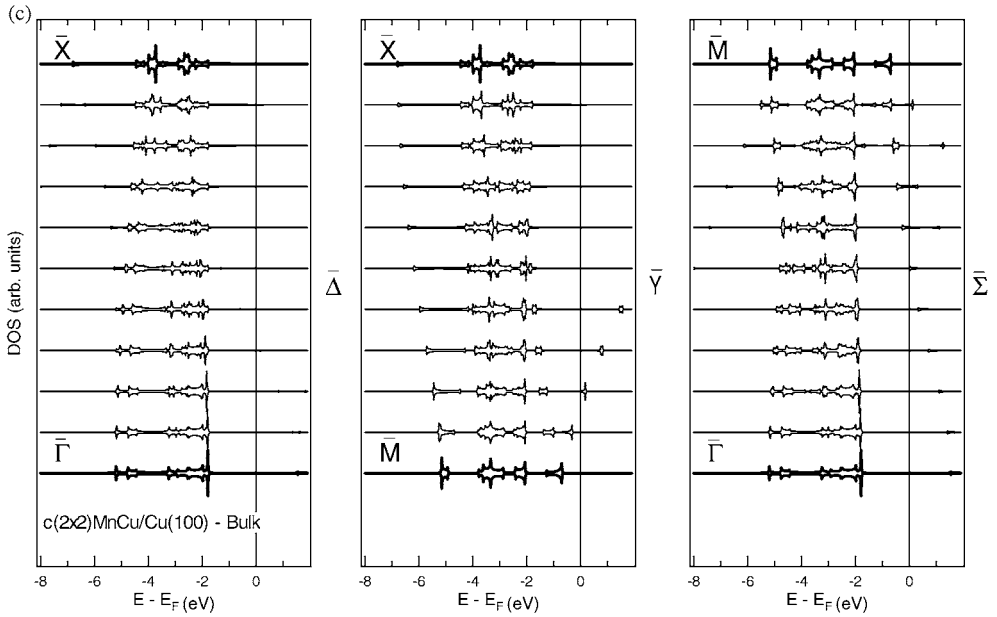

Figure 4. (Continued.)

The effects of folding the BZ can be better understood regarding the bulk DOS of the (1×1)-Cu(100) and (2×2)-MnCu/Cu(100) systems. As can be seen in figure 1, the (2×2)-$\overline{\Sigma}$ direction contains the projections of the (1×1) lines $\overline{\Delta}$ and $\overline{Y}$, the contributions from the (1×1) points $\overline{\Gamma}$ and $\overline{M}$ corresponding to the point (2×2)-$\overline{\Gamma}$. In analogy, the line (1×1)-$\overline{\Sigma}$ is folded onto the (2×2)-$\overline{\Delta}$, so that the point (2×2)-$\overline{X}$ coincides with the middle point of the (1×1)-$\overline{\Sigma}$ direction. Compare now the bulk DOS of figures 2 and 4. At $\overline{\Gamma}$ the bulk valence band of figure 4 separates into two main structures, one centred around -3 eV and the other around -5 eV. The larger width of both subbands with respect to the corresponding ones at the point (1×1)-$\overline{\Gamma}$ is due to the contribution from the point (1×1)-$\overline{M}$. If we follow the evolution of the DOS along the line (2×2)-$\overline{\Delta}$, no bulk bandgap opens in the (2×2) projection; as a consequence, the SSs $\overline{\Gamma_1}$ and $\overline{M_2}$ of Cu(100) are not present at the new surface. However, enhanced intensities are found for the Cu atoms at the two topmost planes in the region that would correspond to the state $\overline{\Gamma_1}$, and a SR dominated by the minority band of Cu_0 can be solved at -4.39 eV in $\overline{\Gamma}$. Similarly, most of the bulk gaps along the line (1×1)-$\overline{Y}$ disappear when it folds onto the (1×1)-$\overline{\Delta}$ leading to the $\overline{\Sigma}$ projection of figure 4.

The largest number of bulk bandgaps of the (2×2) BZ can be found around $\overline{M}$, and consequently most surface features of the valence band concentrate at this point. We showed in our previous contribution [12] that, close to E_F, the proximity of the minority-spin band of Mn induces new states very localized at the MnCu plane; they have almost the same weight in the Mn and Cu atoms, opposite to the minority-spin states of the conduction band. While our previous contribution was focused on the new electronic states in the vicinity of the Fermi edge [12], here we extend our study to a broader region between -2 and -6 eV, where most valence band features specific to the surface alloy lie. The main effect in this energy range is the redistribution of weight of the states, which can be clearly observed in the results of the ARUPS measurements. In figure 5, we show the ARUPS spectra of the surface alloy along the (1×1) symmetry lines $\overline{\Delta}$ and $\overline{\Sigma}$. Comparing them with those of the clean Cu(100) surface, we

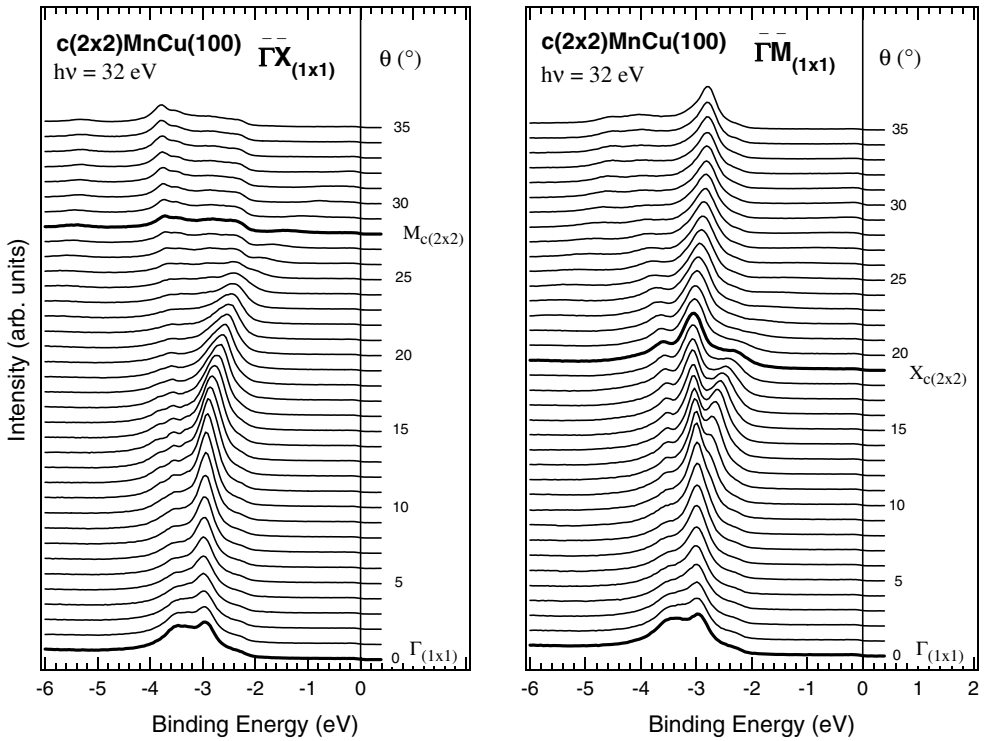

Figure 5. The same as figure 3 for the c(2 × 2)MnCu/Cu(100) surface. The symmetry directions are referred to the (1 × 1) unit cell, although the spectra corresponding to the symmetry points of the (2 × 2) BZ are indicated.

observe that the largest intensities appear at the same binding energy range (namely between −4 and −2 eV), which also corresponds to the highest bulk occupancies. Although there is not a clearly differentiated structure that can be assigned to the Mn-induced states, the shape of the spectra has changed, evidencing the overlap in energy of the valence bands of Mn and Cu. The double peak centred at −3 eV in the clean Cu(100) surface converts into a single peak in the surface alloy as we approach $\overline{\mathrm{M}}$. In the layer-resolved DOS we can appreciate that the origin of this redistribution is mainly due to the spin polarization of the Cu atoms. As in the (1 × 1)-Cu(100) termination, the lower subband between −4 and −6 eV cannot be detected experimentally due to the symmetry selection rules. Most gaps of the bulk projection concentrate in this energy region around $\overline{\mathrm{M}}$. In particular, a state reminiscent of the SS $\overline{\mathrm{X}}_3$ of the Cu(100) surface can be localized at −4.2 eV in $\overline{\mathrm{M}}$, dispersing along both $\overline{\Sigma}$ and $\overline{\mathrm{Y}}$; it has more weight in the Cu_0 atoms than in Mn, and a balanced contribution from the majority-and minority-spin bands. New states originated by the majority-spin band of Mn appear close to the bottom edge of the bulk valence band; they also have an important weight in the majority-spin states of Cu_0, due to the overlap of both d bands. An extended state is centred in $\overline{\Gamma}$ at −5.64 eV, and more localized ones can be solved at different points of $\overline{\Sigma}$.

In table 4 we show the atomic magnetic moments at the two topmost layers of the structure, where the only non-zero values could be found. Notice that all Cu atoms of plane 1 (the first Cu plane below the MnCu layer) are equivalent by symmetry. The Mn atoms carry a giant magnetic moment of 3.90 μ_B, in good agreement with previous *ab initio* calculations [3, 10]. The Cu atoms experience a slight but significant polarization, of the same order of the one

Table 4. Atomic magnetic moments of the MnCu alloyed layer (Mn, Cu_0) and the adjacent Cu plane (Cu_1) at the c(2 × 2)MnCu/Cu(100) surface and at the interface of this surface with a semiinfinite Cu(100) crystal. Units are μ_B.

Atom	Surface	Interface
Mn	3.90	4.05
Cu_0	0.05	0.02
Cu_1	0.01	0.02

found for Cu in Co/Cu and Fe/Cu multilayers [33], and their moment is larger the closer they are to Mn.

It is interesting to compare the surface potential of the CuMn surface to that of Cu(100), shown in table 2. No redistribution of the charge occurs at the Cu(100) surface, except for the small transfer of 0.03 electrons from the sp to the d band at the topmost layer. However, this situation is achieved through the inclusion of a large surface potential. The influence of the surface is different depending on the orbital character of the electrons. The sp electrons, being less localized around the ion cores, penetrate into the vacuum, reducing their kinetic energy [29], which is reflected in the high attractive surface potential. In contrast, the d electrons experience a repulsive potential due to the loss of neighbouring attractive cores. The situation is very similar at the surface alloy for the Cu_0 atoms. However, the Mn atoms feel an attractive surface potential both for the sp and d electrons. In fact, the same attractive surface potential applies for all orbitals of the Cu atoms at layer 1, reflecting more the influence of the bonding to Mn than the presence of the surface.

As a final remark we would like to comment the effects on the electronic structure of the buckling of the Mn atoms. These effects have been analysed through the dependence of the interaction parameters on the interatomic distance (equation (1)), and were not included in our previous study of the surface alloy [12]. When comparing with the former results, the existence of corrugation changes slightly the relative weight and the energy position of the k-resolved states, inducing a splitting of the energy levels. However, the global description of the electronic properties derived from the integrated DOS remains valid. Using the values of the surface potential in table 2, the most relevant difference is the redistribution of charge at the two outermost layers. In the absence of corrugation, there exists a transfer of d electrons from Cu_0 to the underlying Cu atoms. Minor changes can be observed in the magnetic moments: the spin polarization of Cu at layer 1 increases up to 0.02 μ_B, while the moment of Mn is slightly reduced to 3.87 μ_B.

4. The c(2 × 2)MnCu layer embedded in Cu(100)

In the following we study the electronic structures of a c(2 × 2)MnCu two-dimensional alloy embedded in Cu(100) and a MnCu/Cu/MnCu/Cu multilayer. The analysis of these systems is driven by our interest in studying multilayers made of c(2 × 2)MnCu(100) units, which have been already prepared experimentally, and where the Mn atoms preserve their high-spin ground state [11]. In the electronic structure of the c(2 × 2)MnCu surface alloy, it is difficult to separate the surface effects from those originated by the presence of Mn. Although the buried interface may induce specific effects on the electronic structure [34], we will show that it serves to separate the surface features present in the surface alloy from those induced by Mn.

The interface of the system c(2 × 2)MnCu/Cu(100) with a semiinfinite Cu(100) crystal can also be interpreted as a MnCu alloyed layer embedded in Cu. As no difference exists between the upper and lower Cu(100) semicrystals, no corrugation was initially assumed at

the MnCu plane. Figure 6 shows the spin-resolved DOS of the Mn and Cu atoms of the alloyed layer (plane 0) along the high-symmetry lines of the c(2×2) unit cell. As a reference, we also present in the figure the DOS of a Cu atom at any of the immediately adjacent Cu planes (planes 1 and $\bar{1}$, corresponding respectively to the lower and upper semicrystals). No difference is assumed between the two Cu_1 sites of the (2×2) unit cell, both being equivalent by symmetry. Similarly, the mirror symmetry of the interface system around the CuMn plane makes planes 1 and $\bar{1}$ equivalent. Comparing figure 6 with the results on the surface alloy (figure 4), the more relevant changes are the broadening of the DOS at the MnCu layer, due to the increased atomic coordination, and the slight shift of the minority-spin conduction band of Mn. This leads to a slight enhancement of the exchange splitting, of 4.7 eV measured from the total DOS. Also, the embedding of Mn in the Cu lattice makes the distribution of the spectral weights of Mn more similar to the bulk projection. But most features of the surface alloy are present here, indicating that they are characteristic of the c(2×2)-MnCu system, and not surface effects. The Mn atoms exhibit a large spin polarization which induces an important redistribution of the spin charge at the neighbouring Cu atoms. This redistribution is here more evident at the Cu_0 atoms, while the adjacent Cu planes resemble more the bulk than in the case of the surface. If we analyse in detail the k-resolved DOS, there are variations in the spectral weight of the states with respect to the surface alloy, but their position in energy does not change significantly. Only the states induced by Mn at the bottom of the valence band shift slightly to lower energies, probably due to the broadening of the DOS at the interface. The only new states not overlapping the bulk projection can be identified around $\overline{\mathrm{M}}$, very localized at the alloyed layer. They contain the largest contribution of the minority spin of Mn at the valence band, although they have a significant weight on Mn and Cu for both spin directions. The first of these states lies at the bottom of the valence band, and is very extended in the BZ: it disperses from the middle point of $\overline{\mathrm{Y}}$ towards $\overline{\mathrm{M}}$, where it is localized at -5.8 eV; then it follows the line $\overline{\Sigma}$ moving back to lower energies, until it overlaps the bottom bulk s band. The other one disperses along $\overline{\Sigma}$ between -2 eV to E_F, from $\overline{\mathrm{M}}$ to the centre of the line.

In table 4 we show the magnetic moments at the MnCu layer (Mn, Cu_0) and at one of the equivalent Cu atoms of the adjacent Cu planes (Cu_1). The fast damping of the interface effects also observed in the DOS makes the spin polarization at the planes farther away from the interface negligible. When comparing to the MnCu surface alloy, we observe that an increasing number of non-magnetic neighbours of Mn results in an enhancement of its magnetic moment. This is compatible with the reported magnetic moment of Mn impurities embedded in a non-magnetic transition metal [35], where the moment of Mn is over 4 μ_B. On the other hand, the more symmetric structure reduces the differences between the Cu atoms, leading to a more or less uniform polarization for all first neighbours of Mn.

As already mentioned, the above theoretical results correspond to the absence of buckling in the alloyed layer. We investigated the effect of maintaining this corrugation at the interface, considering two extreme cases to position the adjacent Cu layers (planes 1 and $\bar{1}$): either they maintain the same interatomic distance to Mn (case A), or they preserve the distance to the Cu_0 atoms (case B). Both situations are schematically depicted in figure 7. The first case would correspond to a tendency of the Mn atoms to separate from their Cu neighbours in both adjacent planes. In this situation the Mn atoms have two kinds of close neighbours: those in the same layer, and those in the upper and lower planes. The second case will dominate if the pure Cu layers try to adopt the Cu lattice while the MnCu plane keeps its corrugated atomic arrangement. Then the distances to the upper, in-plane and lower neighbours of Mn are all different. The results of our calculations for both cases of corrugation indicate an important redistribution in weight of the states characteristic of the CuMn alloyed layer, specially around the point $\overline{\mathrm{M}}$; although no new feature occurred, the shape of the peaks in the DOS changed,

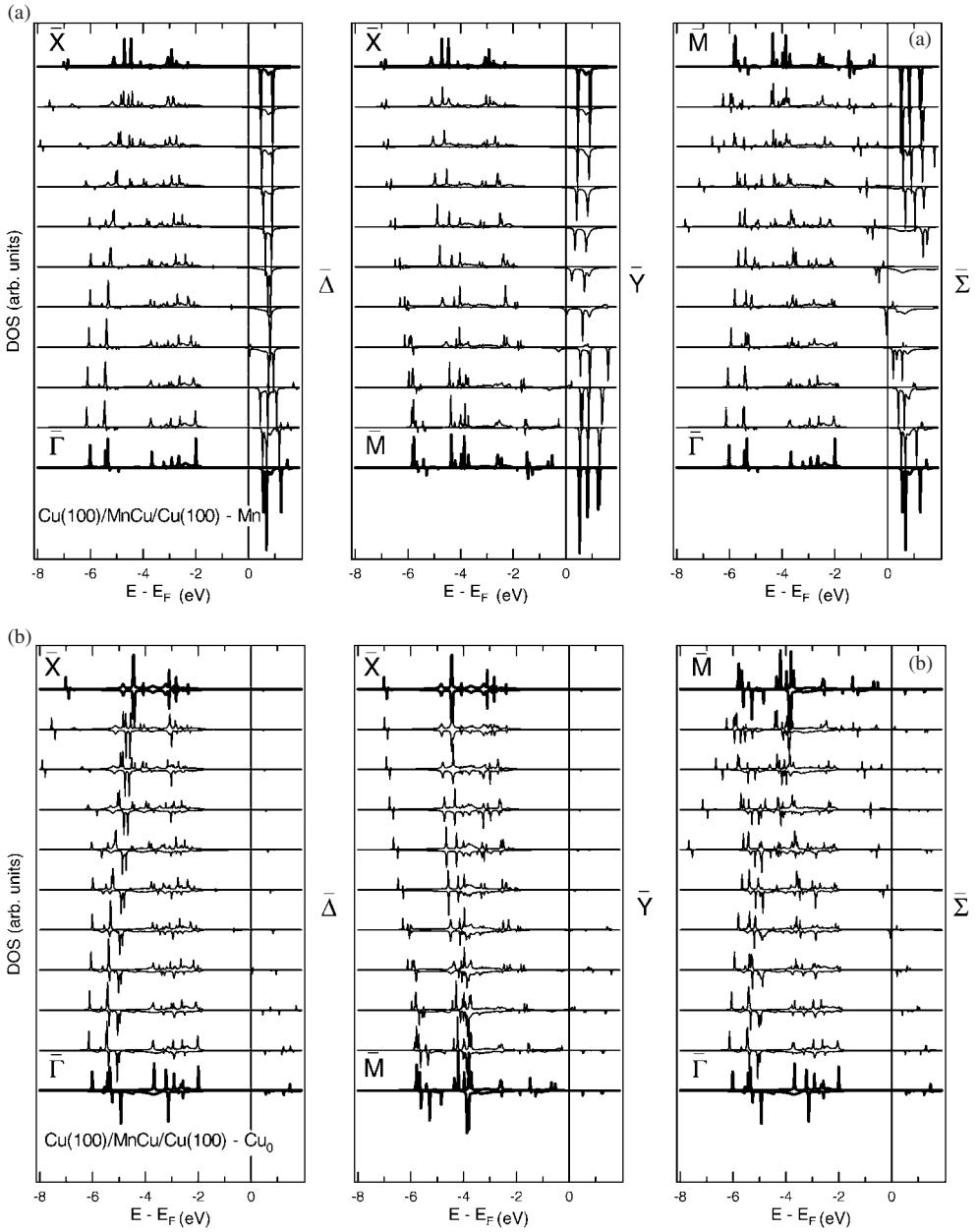

Figure 6. The same as figure 4 for the Mn (a) and Cu (b) sites of the c(2 × 2)MnCu layer embedded in a Cu(100) matrix. Panels (c) correspond to a Cu atom at one of the Cu layers immediately adjacent to the CuMn plane.

mainly due to a splitting of the states and slight shifts in their energy position. Regarding the properties derived from the integrated DOS, no charge neutrality was attained at the interface, specially in case A. This implies the need to modify the interaction parameters with respect to the non-buckled interface, something that did not occur when including the corrugation at the surface. In addition, relevant differences between the two situations modelled were observed.

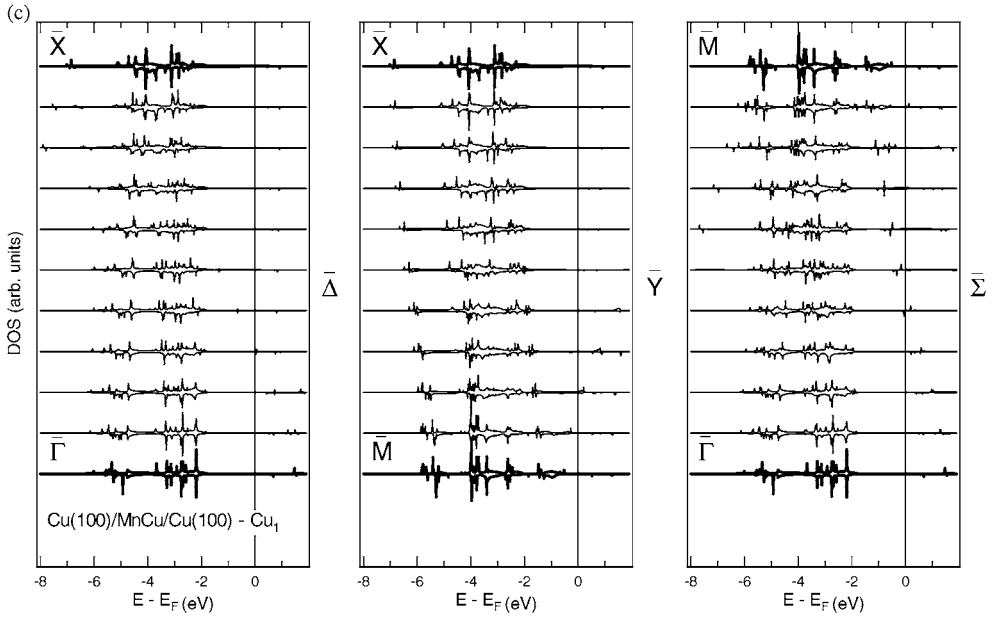

Figure 6. (Continued.)

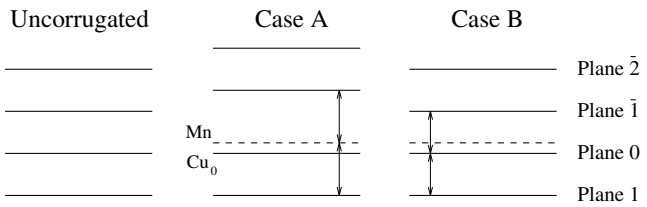

Figure 7. Schematical view of the layer positions at the corrugated interfaces described in the text.

In case A there exists an important redistribution of the charge at the MnCu plane, also affecting the adjacent Cu layers. The Mn atoms lose sp charge, which is transferred to the in-plane Cu neighbours; in turn, these Cu atoms yield d electrons to the adjacent Cu planes. In addition the magnetic moments at the MnCu layer are enhanced, specially that of Mn. It is also interesting to mention that both Cu layers adjacent to the MnCu plane show almost the same electronic properties, as if the mirror symmetry of the structure were determined by the plane defined by the Mn atoms, independently of the positions of the Cu_0 atoms. In contrast, in case B the charge and moments at the MnCu layer remain almost unaffected by the corrugation, the important modifications occurring in the adjacent Cu layer closer to Mn (plane $\bar{1}$). This layer exhibits large differences with respect to plane 1, and in particular the Cu atoms enhance their moment significantly due to a loss of minority spin charge. Although no relevant change in the total DOS of the alloyed layer was observed, an important redistribution of the occupancies between the majority- and minority-spin bands occurs, as if they were trying to fit the additional charge transferred from plane 1.

The ability to form a second $c(2 \times 2)$MnCu surface alloy on top of another one buried under 10 ML of Cu has been demonstrated in a previous work by some of the authors [11].

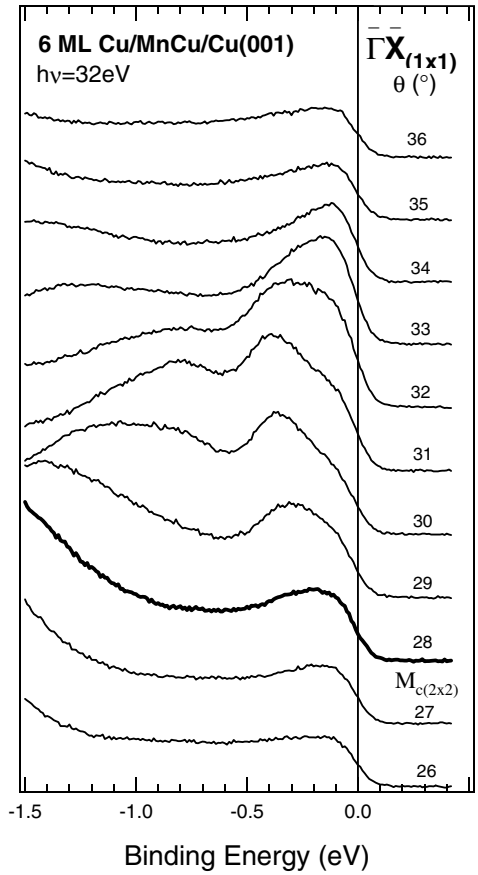

Figure 8. Photoemission spectra of the surface resulting after the evaporation of 6 ML of Cu on c(2 × 2)MnCu/Cu(100). They correspond to the region close to the Fermi edge and around the point (1 × 1)-$\overline{X}$ along the direction $\overline{\Delta}$. The spectrum at $\overline{X} = \overline{M}_{(2\times2)}$ is marked in bold.

As explained in section 2, the formation of the multilayered structures proceeded through the evaporation of 10 ML of Cu on a perfect c(2 × 2)MnCu/Cu(100) surface, followed by the formation of a second c(2 × 2)MnCu on top. The thickness of the spacer was chosen as the thinnest giving a good (1 × 1) LEED pattern with reduced background. Taking into account the fast damping of the surface effects, this thickness seems to be enough to avoid the influence of the new surface on the buried MnCu layer. To explain this in more detail, we will start by analysing the evolution of the ARUPS spectra as Cu is deposited onto the MnCu surface alloy. We will concentrate on the changes measured in the region close to the Fermi edge and around the (1 × 1)-$\overline{X}$ point, where we have already solved experimentally different SSs at the Cu(100) and the c(2 × 2)-MnCu surfaces [12]. In figure 8 we show such a region for a Cu coverage of 6 ML. The existence of a (1 × 1) LEED pattern was checked for this surface. The corresponding spectra should be compared with those corresponding to the clean Cu(100) surface and the c(2 × 2) surface alloy, shown in figure 2 of [12]. When doing this, it is evident that the additional Cu induces changes in the valence band states. The three peaks clearly resolved around the point (1 × 1)-$\overline{X}$ in the MnCu surface, which correspond to Mn-induced features according to the calculated DOS [12], disappear, and a tendency to evolve towards the

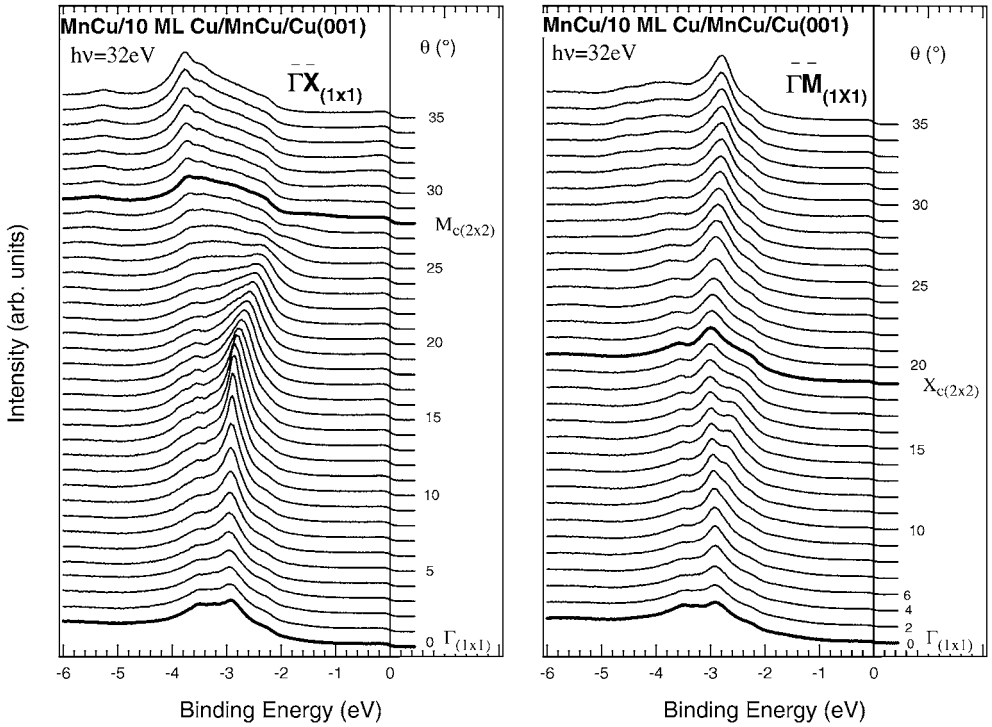

Figure 9. The same as figure 5 for the c(2 × 2)MnCu surface alloy formed on top of 10 ML of Cu covering a c(2 × 2)MnCu/Cu(100) structure.

clean Cu spectra can be observed. However, traces of the states induced by Mn in the surface alloy remain, as if they were still present at the buried interface with Cu. For example, the feature closer to the Fermi edge, located around −0.4 eV in the 30° spectrum of the MnCu surface, can be identified in the surface covered by 6 ML of Cu.

The quality of the (1 × 1)-LEED pattern improved for a coverage of 10 ML of Cu and a second c(2 × 2)MnCu surface alloy was formed. In figure 9 we show the ARUPS spectra of the final bilayered system along the high-symmetry directions. When compared to figure 5 we see the reproducibility of all main features of the spectra, which maintain their shape and energy location for each point of the reciprocal space. This is in accordance with the theoretical results presented here, which evidence the fast damping of the interface effects, and suggest the tendency of the buried MnCu layer to adopt a non-corrugated structure. Complementary studies are needed to better know the magnetism and atomic structure of the multilayers; however, the above results clearly demonstrate the possibility of growing in a controlled way multilayers made of identical two-dimensional c(2 × 2)MnCu.

5. Conclusions

We have presented the electronic structure of a c(2 × 2)MnCu layer as a surface alloy on Cu(100) and embedded within a Cu matrix. The results are governed by the overlap of the valence d bands of Mn and Cu. The high spin moment of Mn induces a spin polarization of the neighbouring Cu atoms, which results in a very different distribution of the electronic states for both spin directions. States characteristic of the alloyed layer can be identified mainly at

the bottom of the valence band and close to the Fermi level, specially around the (2×2)-$\overline{\mathrm{M}}$ point. The spectral weight and the energy position of these states are very sensitive to the corrugation of the MnCu layer.

The main differences between the surface alloy and the c(2×2)MnCu layer buried under Cu correspond to the slight broadening of the DOS (with the subsequent energy shift of the electronic states) and the prediction of change of the magnetic moments. The moment of Mn increases when it is completely surrounded by Cu, as a result of the enhanced coordination of the Mn atoms to non-magnetic neighbours. On the other hand, the moment of the Cu atoms is completely determined by their distance to Mn, the closest distances inducing the largest moments. Accurate measurements of the k-resolved spin-polarized spectra would allow us to observe these variations.

Acknowledgments

This work has been partially financed by the Spanish DGICYT under contracts BFM2000/1330 and PB97-1199. SG acknowledges financial support from the Comunidad Autónoma de Madrid. YH acknowledges financial support from the Spanish Ministerio de Educación y Cultura, and the University of York, UK.

References

[1] Tommes R *et al* 1996 *J. Phys.: Condens. Matter* **8** 10231
[2] Fabricius G *et al* 1995 *Surf. Sci.* **331–333** 1377
[3] Wuttig M, Gauthier Y and Blügel S 1993 *Phys. Rev. Lett.* **70** 3619
[4] Flores T, Hansen M and Wuttig M 1992 *Surf. Sci.* **279** 251
[5] Van der Kraan R G P and Van Kempen H 1995 *Surf. Sci.* **338** 19–30
[6] Wuttig M, Knight C C, Flores T and Gauthier Y 1993 *Surf. Sci.* **292** 189
[7] O'Brien W L and Tonner B P 1995 *Phys. Rev.* B **51** 617
[8] O'Brien W L, Zhang J and Tonner B P 1993 *J. Phys.: Condens. Matter* **5** L515
[9] Rader O *et al* 1997 *Phys. Rev.* B **55** 5404
[10] Eder M, Hafner J and Moroni E G 2000 *Phys. Rev.* B **61** 11492
[11] Huttel Y, Schiller F, Avila J and Asensio M C 2000 *Phys. Rev.* B **61** 4948
[12] Huttel Y, Gallego S, Muñoz M C and Asensio M C 2001 *Surf. Sci.* **482–485** 540
[13] Schiller F, Huttel Y, Avila J and Asensio M C 1999 *Surf. Sci.* **433–435** 434
[14] Wuttig M, Junghans S and Flores T 1996 *Phys. Rev.* B **53** 7551
[15] Wortmann D, Heinze S, Bihlmayer G and Blügel S 2000 *Phys. Rev.* B **62** 2862
[16] Rader O *et al* 1997 *Europhys. Lett.* **39** 429
[17] Binns C and Norris C 1982 *Surf. Sci.* **116** 338
[18] Schiller F, Halilov S V and Laubschat C 2002 *Phys. Rev.* B **65** 184430
[19] Blügel S 1996 *Appl. Phys.* A **63** 595
[20] Huttel Y, Teodorescu C M, Bertran F and Krill G 2001 *Phys. Rev.* B **64** 094405
[21] Slater J C and Koster G F 1954 *Phys. Rev.* **94** 1498
[22] Papaconstantopoulos D A 1986 *Handbook of the Band Structure of Elemental Solids* (New York: Plenum)
[23] Harrison W A 1989 *Electronic Structure and the Properties of Solids* (New York: Dover)
[24] Muñoz M C and López-Sancho M P 1990 *Phys. Rev.* B **41** 8412
[25] Smith J R *et al* 1980 *Phys. Rev.* B **21** 2201
Fabricius G *et al* 1994 *Phys. Rev.* B **49** 2121
[26] Kevan S D *et al* 1985 *Phys. Rev.* B **31** 3348
[27] Euceda A *et al* 1983 *Phys. Rev.* B **27** 659
[28] Wincott P L *et al* 1986 *Surf. Sci.* **178** 300
[29] Pérez-Díaz J L and Muñoz M C 1994 *Phys. Rev.* B **50** 8825
[30] Heinmann P *et al* 1979 *Phys. Rev. Lett.* **42** 1782
Heinmann P *et al* 1979 *Phys. Rev.* B **20** 3059
[31] Hayden A B, Pervant P and Woodruff D P 1995 *J. Phys.: Condens. Matter* **7** 1139

[32] Schiller F, Danzenbächer S and Laubschat C 2001 *Surf. Sci.* **482–485** 442
[33] Samant M G *et al* 1994 *Phys. Rev. Lett.* **72** 1112
Pizzini S, Fontaine A, Giorgetti C and Dartyge E 1995 *Phys. Rev. Lett.* **74** 1470
[34] Dürr H A, Van der Laan G, Spanke D, Hillebrecht F U and Brookes N B 1997 *Phys. Rev.* B **56** 8156
Richter M C *et al* 2001 *Phys. Rev.* B **63** 205416
[35] Blügel S, Weinert M and Dederichs P H 1988 *Phys. Rev. Lett.* **60** 1077
Schieffer P, Krembel C, Hanf M C and Gewinner G 1998 *Phys. Rev.* B **57** 1141